Translucent Acrylic Nanocomposites Containing Anisotropic Laminated Nanoparticles Derived from Intercalated Layered Silicates

FRANK DIETSCHE, YI THOMANN, RALF THOMANN, ROLF MÜLHAUPT

Albert-Ludwigs-Universität Freiburg, Institut für Makromolekulare Chemie und Freiburger Materialforschungszentrum, Stefan-Meier-Strasse 21, D-79104 Freiburg i. Br., Germany

Received 26 October 1998; accepted 3 June 1999

ABSTRACT: New acrylic nanocomposites consisting of methyl methacrylate (MMA)/*n*-dodecylmethacrylate (LMA) copolymers and intercalated layered silicates were prepared. The silicates were based upon bentonite which was rendered organophilic by ion exchange with *N,N,N,N*,-dioctadecyl dimethyl ammonium ions. Morphological, thermal, mechanical, and optical properties were examined as a function of both organophilic bentonite and LMA content. Addition of LMA improved the compatibility between the layered silicate and the acrylic matrix, thus promoting bentonite intercalation and formation of anisotropic laminated silicate nanoparticles of an average diameter of 18 nm, average length of 450 nm, and interlayer distance of 4.8 nm, as determined by WAXS, TEM, and AFM. Addition of 2–10 wt % of intercalated layered silicate accounted for improved stiffness/toughness balance, higher glass temperature, and enhanced thermal stability, with respect to the properties of the corresponding MMA/LMA copolymer. As a result of the addition of LMA, translucent acrylic nanocomposites were obtained. © 2000 John Wiley & Sons, Inc. J Appl Polym Sci 75: 396–405, 2000

Key words: acrylate; copolymer; bentonite; layer; silicate

INTRODUCTION

An important objective in the development of acrylic engineering materials is to achieve matrix reinforcement without sacrificing optical clarity, easy processability, and impact strength. Most conventional reinforcing agents, such as fibers and fillers, are fairly large and scatter light, thus reducing light transmittance.[1] Several attempts have been reported to incorporate nanofillers into a polymer matrix.[2,3] Efficient particle dispersion, preferably of particles with a large length/diameter ratio (aspect ratio), combined with good interfacial adhesion is the prime requirement for achieving matrix reinforcement. Due to the large surface area of nanoparticles, strong interparticular interactions make dispersion of the nanofiller particles very difficult. Large clusters of nanoparticles are well known to be the reason for premature crack propagation occurring at small mechanical stresses. Moreover, thixotropy of such nanoparticle assemblies results in high viscosities at low shear rates which are detrimental to acrylate casting processes applied in the production of acrylic sheets. These problems have limited the use of nanoparticles such as pyrogenic silica. Even though polymerization in the presence of pyrogenic silica improves dispersion, most researchers were able to incorporate only rather small amounts, typically less than 10 wt %, without achieving significant matrix reinforcement.[4–7]

Correspondence to: R. Mülhaupt.

Journal of Applied Polymer Science, Vol. 75, 396–405 (2000)
 CCC 0021-8995/00/030396-10

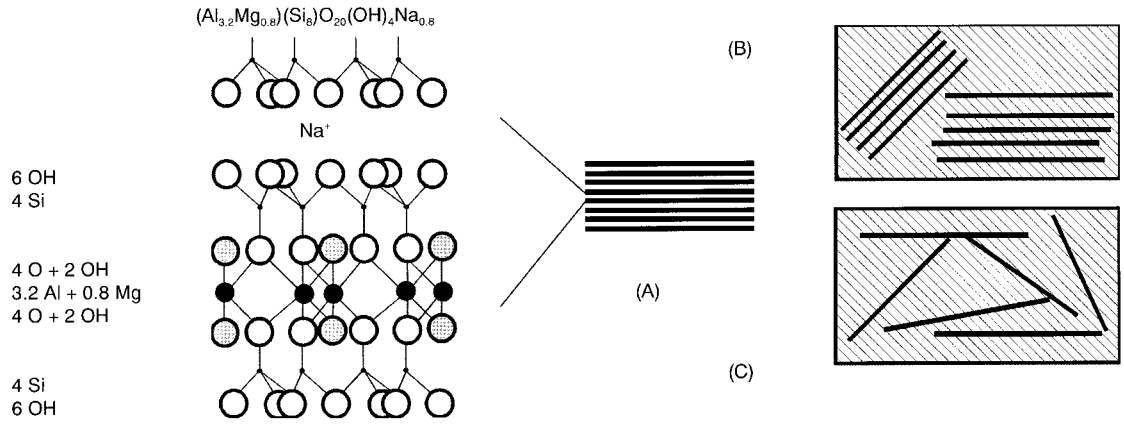

Figure 1 (A) Bentonite and (B) the corresponding intercalated and (C) exfoliated polymer nanocomposite.

Anisotropic nanoparticles with high aspect ratios are of particular interest in matrix reinforcement. However, most anisotropic nanoparticles with large aspect ratios require special precautions during compounding because of health hazards associated with the inhalation of such particles. Thus, preferably, nanoparticles would be prepared *in situ* during processing. Sol/gel technology has been applied to produce a large array of organic–inorganic hybrid materials based upon mainly isotropic nanoparticles.[2,3] Sol/gel processes involve the hydrolysis of alkoxy silanes and metal alkoxides. This process is not compatible with conventional methyl methacrylate (MMA) casting.

A more attractive route to *in situ* formation of nanoparticles with large aspect ratios was found in the intercalation of organophilic clay, which are dispersed during intercalation into their nanoscale building blocks, that is, anisotropic layered silicates with a very high aspect ratio. This technology was reviewed by Akelah,[8] Pinnavaia et al.,[9] Giannelis,[10] and Lagaly.[11] Layered silicates such as clay are readily available minerals.

Bentonites are composed of montmorillonite which consists of a center sheet of octahedral alumina sandwiched in between two silica sheets. Since part of the trivalent aluminium ions are substituted by divalent magnesium ions, the individual layers are charged negatively. As illustrated in Figure 1, the countercations, predominantly sodium or potassium, are located in the interlayer galleries. Intercalation of these layered silicates is achieved by means of exchange of the Na^+ gallery ions with quarternary ammonium ions containing at least one long *n*-alkyl substituent. Ion exchange renders the silicate layers organophilic and permits swelling in hydrophobic media such as acrylate monomers. Intercalation is accompanied by a significant increase in interlayer spacing between individual silicate layers. Once complete exfoliation of the individual silicate layers is achieved, no interlayer spacings can be detected by means of wide-angle X-ray scattering (WAXS). A schematic representation of bentonite and the two types of polymer nanocomposites are illustrated in Figure 1.

Nanocomposite formation has been achieved with various polymers, for example, epoxy resins,[12,13] polyamides,[14] polypropylene,[15,16] and polyacrylates.[17–19] Remarkable features of polymeric nanocomposites based upon intercalated and exfoliated layered silicates are increased stiffness without sacrificing toughness. This is important for the production of lightweight automotive parts. Moreover, nanocomposites exhibit gas barrier properties useful in packaging applications. Most likely due to limited oxygen and gas permeabilities, nanocomposites enhance fire retardancy.[10,20] It was well known that compatibility between organophilic layered silicates and a polymer or a monomer, respectively, plays a key role. In polyamide nanocomposites, interfacial adhesion is achieved via covalent coupling using protonated aminocarboxylic acid monomers during anion exchange in order to attach amino endgroups of polyamide chains to the layered silicate surface.[21] The compatibility of layered silicates with styrene and MMA was improved by adding ammonium-functionalized styrene,[22] ammonium-functionalized methacrylate, or poly(MMA) (PMMA) containing pendent ammonium

cations.[18] Recently, PMMA nanocomposites were obtained by using emulsion polymerization,[17] where the PMMA emulsion was added to a water-swollen Na^+–montmorillonite in the presence of sodium dodecylsulfate (SDS). Although small (1.28–1.73 nm) interlayer distances were detected, these nanocomposites showed a higher Young's modulus (4.89 GPa) and high tensile strengths (62 MPa) with respect to nonfilled PMMA. One purpose of our research was to investigate the role of compatibilization between intercalated layered silica derived from sodium bentonite via ion exchange with *N,N,N,N*,-dioctadecyl dimethyl ammonium (DDM) chloride and subsequent swelling with MMA, using the dodecyl methacrylate (LMA) comonomer as a compatibilizer. Morphological, thermal, mechanical, rheological, and optical properties were investigated as a function of both organophilic bentonite–DDM and LMA content.

EXPERIMENTAL

Materials

Organophilic bentonite (bentonite–DDM) containing DDM ions (DDM, 0.16 g tenside/g) with particle sizes of 1–5 μm and density of 1.8 g/cm^3 was supplied by Süd-Chemie AG (Moosburg, Germany). MMA was obtained from Röhm AG (Darmstadt, Germany) and used without further purification. Polymerizations were initiated by a catalyst from Röhm, consisting of dioctylphthalate/dibenzoylperoxide (DBP), at room temperature.

Preparation of Bentonite Intercalated PMMA/LMA Copolymer

Sodium–bentonite, ion-exchanged with DDM, was suspended in the amount of LMA required to afford the MMA/LMA/bentonite–DDM ratios listed in Table I. Swelling was performed for the duration of 1 h at room temperature. The resulting highly viscous paste was diluted with MMA and sonicated for the duration of 30 min using a Bandalin RK 52 sonicator equipped with a water bath. Under an argon atmosphere, this mixture was transferred into a mold to produce sheets of 2- or 4-mm thickness. Polymerizations were carried out at room temperature using dibenzoylperoxide in dioctylphthalate as an initiator (2–4 wt % with respect to monomer). Polymerization was

Table I Mechanic and Thermic Behavior of Bentonite–DDM Nanocomposites

Polymer/ Nano-composite	MMA (wt %)	LMA (wt %)	Bentonite–DDM (wt %)	Izod Impact Strength (kJ/m^2)	T_g (°C)[a,b]	Young's Modulus (MPa)	Light-Transmittance Coefficient (cd/m^2 lx)	Elongation at Break (%)	Interlayer Distance, d_{001} WAXS/TEM (nm)	TGA Temperature (°C)[c]
PMMA	100	0	0	1.3 ± 0.2	110[b]	3300 ± 70	0	2.3 ± 0.4	—	255
P5	95	5	0	6.7 ± 0.3	85[a]	3100 ± 70	0	5.6 ± 0.6	—	252
P10	90	10	0	8.1 ± 0.3	72[a]	2500 ± 60	0	8.6 ± 0.6	—	249
P20	80	20	0	—	48[a]	—	0	—	—	244
NC8/5	87	8	5	0.7 ± 0.1	78[a]	4370 ± 80	0.8 ± 0.2	2.1 ± 0.4	5.8–∞	252
NC10/5	85	10	5	0.9 ± 0.1	76[a]	3890 ± 60	0.6 ± 0.2	3.8 ± 0.3	6.3–∞	251
NC15/5	80	15	5	1.5 ± 0.2	60[a]	3100 ± 60	—	4.1 ± 0.5	6.2–∞	253
NC10/10	80	10	10	0.9 ± 0.2	80[a]	4030 ± 50	0.9 ± 0.2	3.3 ± 0.3	5.1–∞	265
NC15/10	75	15	10	0.9 ± 0.2	68[a]	3830 ± 80	0.8 ± 0.2	2.0 ± 0.4	5.3–∞	261
NC15/15	70	15	15	0.6 ± 0.2	74[a]	3750 ± 50	8.2 ± 0.2	3.2 ± 0.5	4.8–∞	267

[a] Determined by DSC using a heating rate of 10°C/min.
[b] Determined by dynamic mechanical analysis at a heating rate of 5°C/min.
[c] Thermogravimetric analysis under air; temperature at which 10 wt % weight loss was observed.

performed in bulk at 80°C for 5 h. The reaction was monitored via heat evolution. Residual MMA was removed by heating to 100°C for 12 h in an oil pump vacuum. High conversion of MMA and LMA was monitored by the disappearance of the characteristic monomer ^{1}H-NMR vinyl signals at 4.6 and 6.3 ppm. After extracting the copolymers with boiling hexane for 13 h, only 0.1 wt % of the initiator residue (dioctylphthalate) was detected by NMR.

WAXS

The degree of swelling and the interlayer distance were studied using WAXS with an image-plate system with CuKα radiation (λ = 1.5418 nm) and a scanning time of 500 s.

Transmission Electron Microscopy (TEM)

The morphology of the samples was examined using TEM with a Zeiss EM 902 and 80 keV acceleration voltage. Ultrathin specimens of 30–50 nm were cut at room temperature using an ultramicrotome (Ultracut E, Reichert & Jung) equipped with a diamond knife. Ultrathin sections were analyzed without staining.

Atomic Force Microscopy (AFM)

AFM experiments were performed using a Nanoscope III scanning probe microscope (Digital Instruments Inc.). The height and phase images were obtained simultaneously while operating the instrument in a tapping mode under ambient conditions. We used commercial Si cantilevers with force constants of 13–70 N/m. Images were taken at the fundamental resonance frequency of the Si cantilever, which was typically around 300 kHz. Typical scan speeds during recording were 0.3–1 line/s using scan heads with a maximum range of 170 $\times$ 170 μm or 16 $\times$ 16 μm. All images were taken with a driving amplitude $A_0 \approx 60$ nm and a set-point amplitude of $A_{sp} \approx 40-48$ nm. The phase images represent variations of the relative phase shifts (i.e., the phase angle of the interacting cantilever relative to the phase angle of the freely oscillating cantilever at the resonance frequency). The flat surfaces were obtained by cutting the sample with a Diatome diamond knife at ≈ -130°C and using a cryomicrotome.

Phase detection allows one to detect shifts in phase angles of vibration when the oscillating cantilever interacts with the sample surface. Phase imaging (i.e., image contrast related to the phase shifts) has been shown to provide enhanced image contrasts, especially for heterogeneous surfaces. The image contrast can result from different surface hardness, tip-surface adhesion, or some surface contamination such as a water layer condensed from air at the ambient condition. Phase imaging can also be affected by sharp edges over which the tip scans.

Measurement of Dynamic Moduli and Tensile Test

Mechanical properties such as the Young's modulus, yield stress, tensile strength, and elongation to break were measured on samples (60 $\times$ 12 $\times$ 4 mm) using stress/strain testing according to DIN 53455 with a Zwick 4202 tensile tester and crosshead speed of 1 mm/min. At least seven samples were measured to assure reproducibility. Notched Izod impact strength was measured using a Zwick 5102 pendulum impact tester according to Izod ISO 180 on a specimen of 60 $\times$ 12 $\times$ 2 dimension using a 2 $\times$ 2.5-mm notch. The dynamic mechanical properties were measured using a Rheometrics RSII solids analyzer and a dual-cantilever specimen (50 $\times$ 6 $\times$ 3 mm) at a frequency of 1 Hz and amplitude of 0.1%. Temperature was varied between -100 and 120°C using a 5°C/min heating rate.

Measurement of Light Transmittance

The light transmittance of the polymer samples were measured on specimens of 80 $\times$ 40 $\times$ 4 mm using a method according to DIN 52348 from Röhm AG (photometer 550 Polytec combined with program named Leuco). The standard deviation was determined to be $<$5%.

Thermogravimetry (TGA) and Viscosity

TGA investigations were recorded on a Netzsch simultaneous thermoanalyser (STA 409) controlled by a Netzsch TASC 412/2 unit. A nitrogen or air atmosphere (flow: 150 mL/min) and a heating rate of 5°C/min were employed. Viscosities were measured using a digital Brookfield DV-II viscometer and viscosity calibration by 5000 mPas.

Characterization of Copolymer–Bentonite Nanocomposites (NMR, GPC, DSC)

^{1}H- and ^{13}C-NMR spectra were recorded on a Bruker ARX 300 spectrometer operating at 300 MHz for ^{1}H and 75.4 MHz for ^{13}C, using TMS as

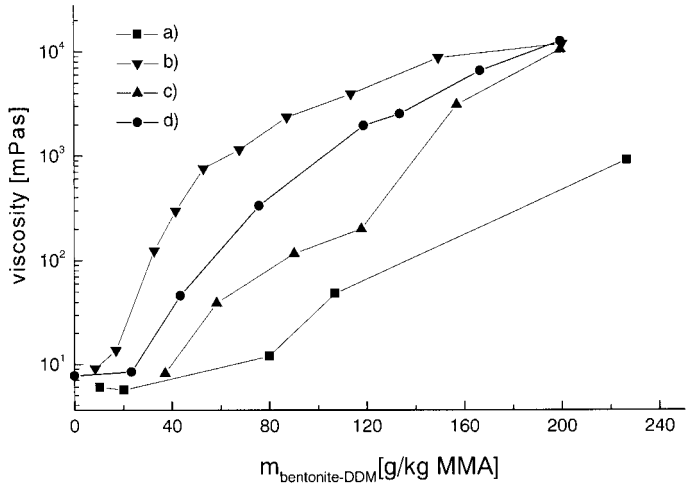

Figure 2 Viscosity of the MMA/LMA/bentonite–DDM mixture prior to polymerization: (a) no LMA; (b) weight ratio 4/3; (c) weight ratio 1/1; (d) weight ratio 3/4 of bentonite–DDM/LMA.

an internal standard in $CDCl_3$ at ambient temperature. Molar masses and molar mass distributions were determined by gel permeation chromatography (GPC) using a combination of 10^5, 10^3, and 100 nm PL columns (Polymer Laboratories) and chloroform as a solvent at ambient temperature. Molar masses were referenced to polystyrene standards prepared by anionic polymerization. Thermal properties were measured by differential scanning calorimetry (DSC) using a Perkin–Elmer DSC-7 at 10 and 20°C/min heating and cooling rates. To assure identical thermal histories, all samples were heated to 150°C, cooled, and heated again to determine glass transitions during the second heating cycle.

RESULTS AND DISCUSSION

Several families of acrylic nanocomposites were prepared by free-radical bulk polymerization of MMA or MMA/dodecyl methacrylate (abbreviated as LMA, lauryl methacrylate) mixtures initiated at room temperature using dibenzoylperoxide in the presence of organophilic layered silicates (bentonite–DDM), which were prepared by aqueous ion exchange of sodium bentonites with DDM chloride.

Compositions of the obtained acrylic nanocomposites and their properties are listed in Table I. The nonfilled polymer samples are referred as P, where the first number corresponds to wt % LMA. The nanocomposite samples are listed as NC with the first number being equivalent to the wt % LMA in the copolymer and the second number being equivalent to the total wt % of bentonite–DDM. All copolymers, recovered from the nanocomposite using solvent extraction, had number-average molecular masses around 250–290,000 g/mol with polydispersities of $M_w/M_n = 2.3$. With increasing content of bentonite–DDM, the polydispersities rose to 2.5.

Intercalation of PMMA/LMA Copolymers in Bentonite

Organophilic bentonites and hectorites are widely applied as thixotropic additives in coatings. Bentonites belong to the smectite group of clay minerals, also known as montmorillonite of the general formula $(Al_{3.2}Mg_{0.8})Si_8O_{20}(OH)_4Na_{0.8}$. In montmorillonite, the individual layers are composed of a center alumina/magnesia sheet sandwiched in between two silica sheets. When part of the trivalent aluminum ions are substituted by divalent magnesium ions, the layer contains a negative surface charge which is compensated by sodium or calcium ions located in the interlayer gallery. The solvation of such interlamellar ions accounts for the well-known water swelling of clay minerals. When sodium ions are exchanged using quarternary ammonium-based surfactants such as DDM chloride, individual layers are rendered hydrophobic and the ionic interlamellar interactions are reduced. Therefore, monomers such as MMA can penetrate into the interlayer

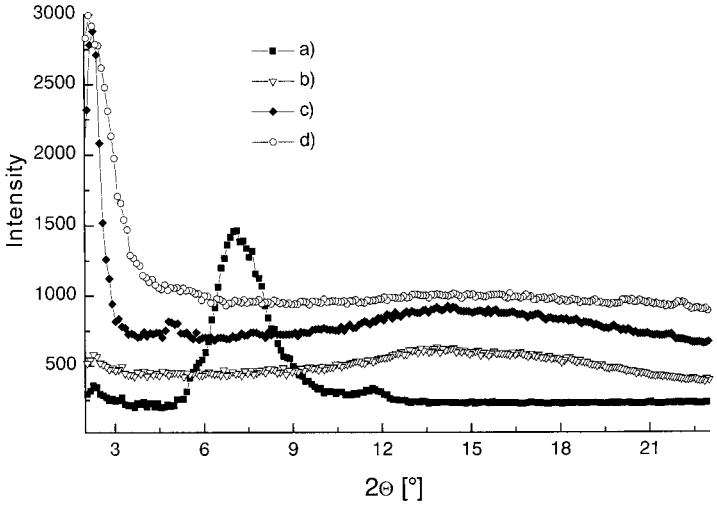

Figure 3 Wide-angle X-ray diffraction of (a) PMMA/bentonite–DDM, (b) P10, (c) NC10/5, and (d) NC10/10.

galleries. In fact, as is apparent from Figure 2, swelling with MMA, as evidenced by the viscosity buildup of bentonite–DDM/MMA suspensions containing 1–10 wt % bentonite–DDM, was rather poor due to the lack of compatibility. Swelling was improved drastically when LMA was added together with MMA. Obviously, the *n*-dodecyl group is much more compatible with the DDM-functionalized layered silicates. When the content of the bentonite–DDM/LMA was varied from 1 to 20 wt %, viscosity increased from 10 to 15,000 mPas. At a bentonite–DDM/LMA weight ratio of 4/3, the viscosity showed a maximum (Fig. 2). Above 15 wt % bentonite–DDM content, even when the LMA content was increased, the high viscosity prevented transfer of the pastelike mixture into the mold. Therefore, the bentonite–DDM content was varied between 0 and 15 wt %.

Detection of Interlayer Distance by WAXS

The role of swelling and separation of the interlayers was monitored using WAXS. Typical WAXS traces for the MMA/LMA copolymer, bentonite–DDM, and bentonite–DDM-based composites are displayed in Figure 3.

MMA failed to afford substantial swelling, as evidenced by a small interlayer distance of 0.8–2 nm, which is very similar to that of pure bentonite–DDM in the absence of MMA. When LMA

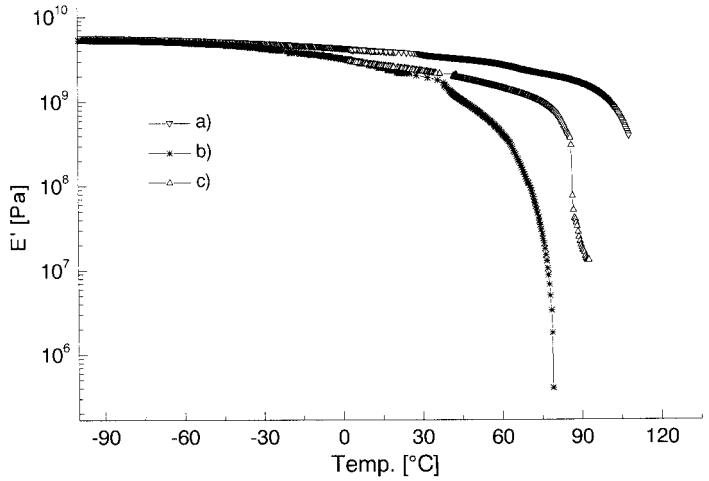

Figure 4 Dynamic mechanical analysis of PMMA, P10, and NC10/10.

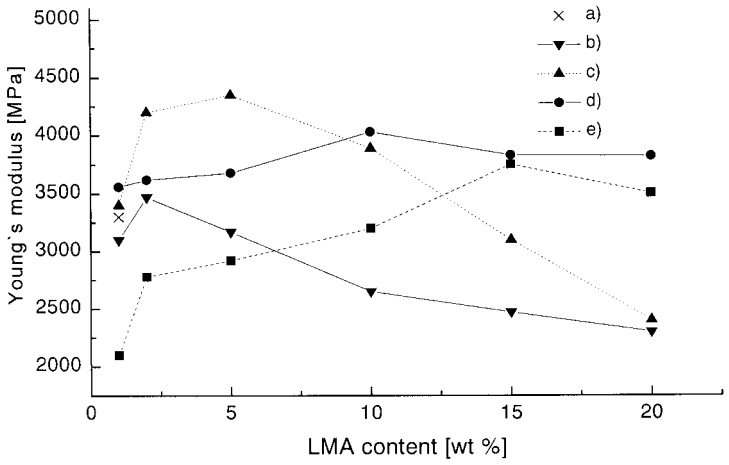

Figure 5 Young's modulus as a function of bentonite–DDM and LMA content: (a) PMMA; (b) 2 wt %, (c) 5 wt %, (d) 10 wt %, and (e) 15 wt % bentonite–DDM.

was added together with MMA, the bentonite–DDM interlayer distance increased drastically from 4.8 to >15 nm by WAXS. Preferably, bentonite–DDM was swollen with LMA prior to MMA addition. The equilibrium state of intercalation was found for LMA at 5 wt % and for MMA at 1.5 wt % after 1 day swelling at room temperature.

Study of Mechanical and Thermal Properties of Nanocomposites

The bentonite–DDM-based PMMA and MMA/LMA copolymer nanocomposites exhibited rather unusual thermal and mechanical properties. Incorporation of LMA into PMMA introduced an internal plasticizer which accounted for the lowering of the glass temperature and the modulus of elasticity with increasing LMA content. When bentonite–DDM was added together with MMA/LMA, both the stiffness and glass transition temperature increased. This is illustrated in Figure 4, which displays the dynamic mechanical analysis of PMMA, copolymer P10, and nanocomposite NC10/10. Probably, the LMA, which was added prior to MMA addition, was polymerized preferably at the silicate interface, thus preventing plastification of the PMMA.

Similar behavior was observed when examining the mechanical properties listed in Table I

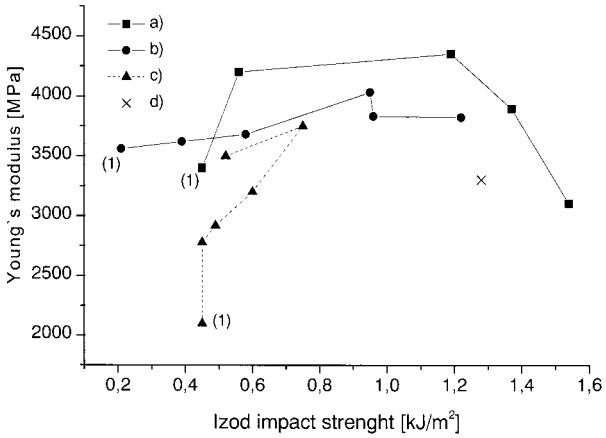

Figure 6 Stiffness/toughness balance expressed by Young's modulus and notched Izod impact strength for various nanocomposites, bentonite–DDM-filled copolymers with increasing (left to right) LMA weight content: (a) 5 wt %, (b) 10 wt %, and (c) 15 wt % bentonite–DDM; (d) PMMA.

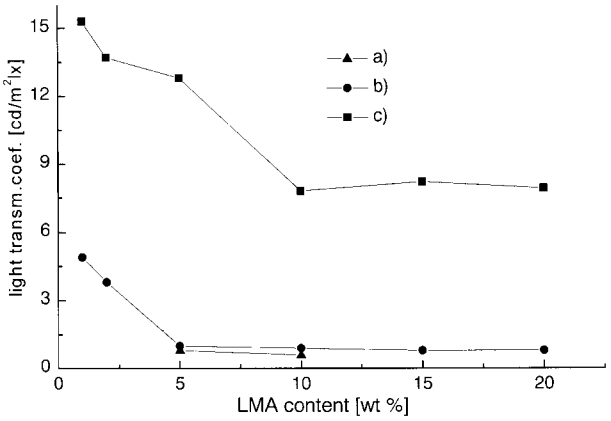

Figure 7 Light transmittance of bentonite–DDM-filled copolymers: (a) 5 wt %, (b) 10 wt %, and (c) 15 wt % bentonite–DDM and variable LMA content.

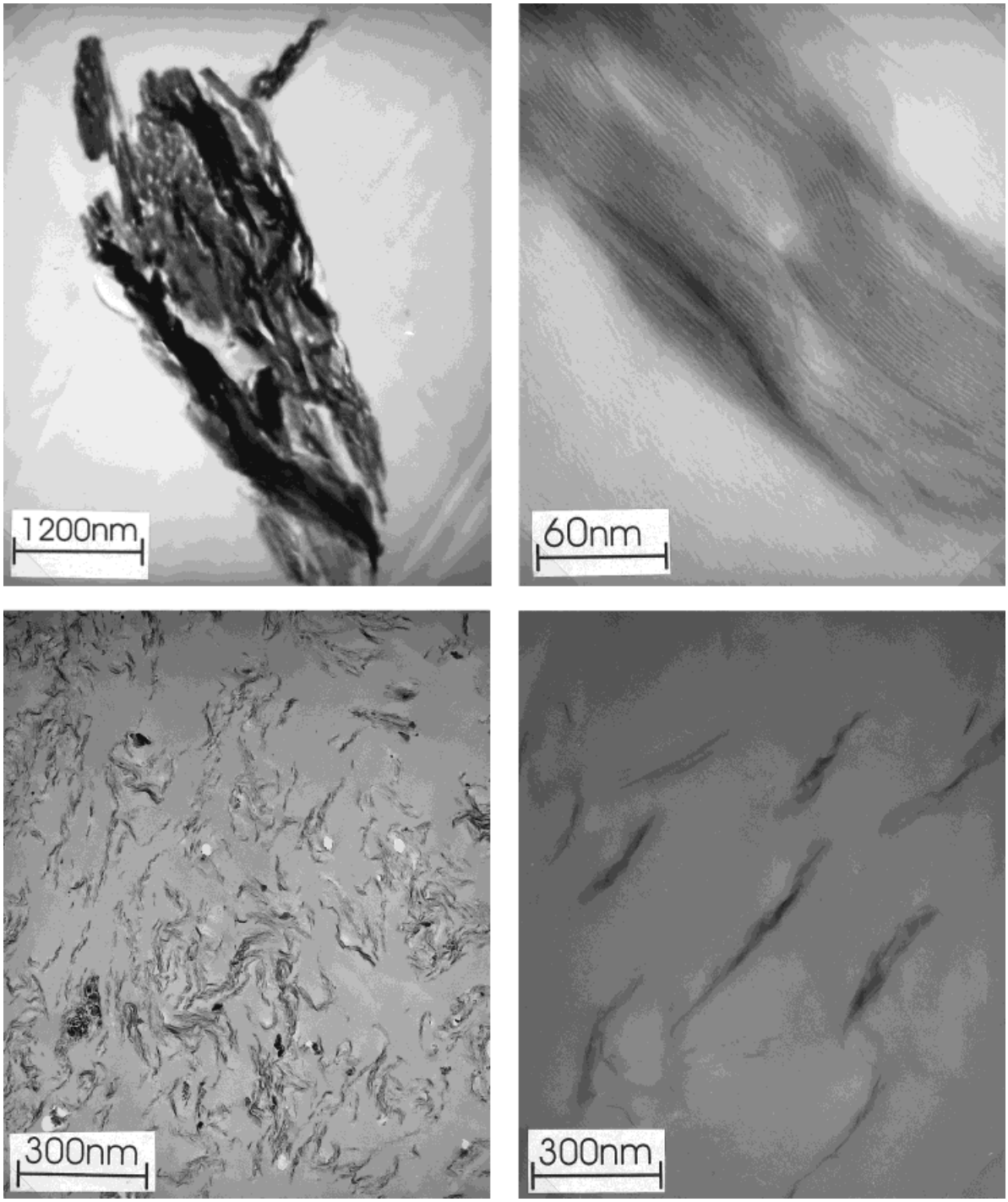

Figure 8 Transmission electron micrograph of unstained MMA/LMA copolymer–bentonite–DDM composites: (a) NC0/10; (b,c) NC15/15; (d) NC10/5.

and Figure 5. While all nanocomposites were rather soft at an LMA content exceeding 5 wt %, LMA contents of <5 wt % accounted for substantial improvements in toughness. At 10 wt %, the Young's modulus increased from 2500 to 4030 MPa. It was possible to balance stiffness and notched Izod impact strength by adjusting the ratio of MMA/LMA at a given bentonite–DDM

content. As is apparent from Figure 6, it is possible to enhance the stiffness of the MMA/LMA copolymers without sacrificing the impact strength. In comparison to PMMA, the toughness/stiffness balance of the nanocomposites was improved.

Light-Transmittance Test

For the development of acrylic materials, it is important to achieve matrix reinforcement combined with enhanced toughness without affecting optical clarity. However, PMMA-based nanocomposites and MMA/LMA nanocomposites with a bentonite–DDM content exceeding 15 wt % were found to be opaque as shown in Figure 7. Light-transmittance coefficients from 0 to 1.0 reflect optical clarity, whereas values exceeding 1.0 indicate the presence of larger structures which scatter light. Interestingly, LMA addition proved to be an excellent tool to tailor translucent nanocomposites. In Figure 7, light transmittance is displayed for PMMA and nanocomposites with variable LMA and bentonite–DDM content. Similar to the improvements of the mechanical properties, the best property combination was achieved with a bentonite–DDM content of 10 wt % and an LMA content of 10 wt %.

Dispersibility of the Bentonite in PMMA/LMA Copolymers

To understand the origins of the unusual mechanical and optical properties, the morphology was examined using TEM and AFM. TEM images of PMMA- and MMA/LMA-based nanocomposites are displayed in Figure 8 and show the presence of anisotropic laminated nanoparticles derived from intercalated bentonite–DDM, in the presence of LMA. It is apparent from Figure 8(a) that pure MMA did not intercalate bentonite–DDM and form laminated nanoparticles, probably due to incompatibility between the PMMA matrix and the bentonite–DDM. There was no evidence for the formation of fully exfoliated nanocomposites, even at high contents of LMA. At a bentonite–DDM content exceeding 10 wt %, large clusters were observed. Such supramolecular assemblies are likely to account for a high viscosity of the suspensions. Interestingly, even samples with high light transmittance contained fairly large assemblies of the layered silicates. Typically, the average diameter of anisotropic laminated nanoparticles was 18 nm, and the average length, 450 nm. Obviously, intercalation of silicate layers with the MMA/LMA copolymers may account for the matching refractive indices of the copolymers to that of the intercalated copolymer-modified layered silicates.

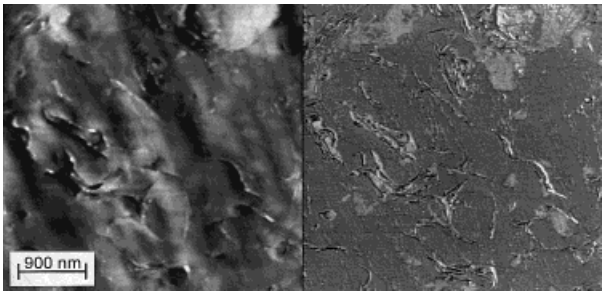

Figure 9 Tapping mode AFM images: (left) height image and (right) phase image, with scan range 4.23 μm, of NC10/5.

AFM images of MMA/LMA-based nanocomposites are displayed in Figure 9, illustrating the dimension and orientation of the structured nanoparticles. Like the TEM images, these show laminated nanoparticles of 400 nm in length and 5–10 nm in diameter. An advantage of AFM imaging is the relatively high phase contrast,[23] between the hard (dark) matrix and the soft (light) silicate particles, of the nanocomposites.

Many publications on nanocomposites assume glasslike rigidity of the layered silicate. In contrast, both TEM and AFM studies clearly indicate that the resulting structures are very soft with respect to the polymer. Upon exposure to mechanical stresses, anisotropic particles can orient to form nanovoids which are very effective stress concentrators. This process can dissipate energy at the crack tip throughout the sample volume. Moreover, upon straining, the individual layers of the larger superstructure undergo shearing, similar to processes typical for metals. Therefore, many intercalated structures with fairly large superstructures give much better impact performance with respect to fully exfoliated nanocomposites. Investigations of the micromechanical processes occurring during the fracture of nanocomposites will be reported elsewhere in even more detail.

Another striking feature of the MMA/LMA-based nanocomposites was their enhanced flame retardancy. Although 10–15 wt % bentonite–DDM was not sufficient to prevent combustion, the burning nanocomposite did not produce droplets of the burning polymer. This may be an at-

tractive route to design novel flame-retardant additives which give improved mechanical properties without sacrificing processability and optical properties.

CONCLUSIONS

Improvement of the compatibility between MMA/LMA copolymer matrix and DDM functional layered silicates represents the key to the formation of novel families of acrylic nanocomposites with an improved stiffness/toughness balance without sacrificing processability in sheet molding and light transmittance. Interfacial interactions also account for enhancement of the glass transition temperature and stiffness because the dodecyl side chains of the internal plasticizer are immobilized on the silicate surfaces and prevent plastification of the matrix. This compatibilizer concept is widely applicable to several other nanocomposite families, as will be presented in other publications.

REFERENCES

1. Handbook for Plastics; Katz, H. S.; Milewski, J. V., Ed.; Van Nostrand Reinhold, New York, 1987.
2. Mascia, L. Trends Polym Sci 1995, 3(2), 61.
3. Schmidt, H. K. In Polymers and Other Advanced Materials; Prasad, N.; Mark, J. E.; Fai, T. J., Eds.; Plenum: New York, 1995; p 611.
4. Hergeth, W. D.; Steinau, U. J.; Schmutzler, K. Polymer 1989, 30, 254.
5. Abramoff, B.; Covinio, J. J Appl Polym Sci 1992, 46, 1785.
6. Frisch, H. L.; Mark, J. E. Chem Mater 1996, 8, 1735.
7. Hergeth, W. D.; Starre, P.; Schmutzler, K. Polymer 1988, 29, 1323.
8. Akelah, A. In Polymers and Other Advanced Materials; Prasad, N.; Mark, J. E.; Fai, T. J., Eds.; Plenum: New York, 1995; p 611.
9. Pinnavaia, T. J.; Lan, T.; Wang, Z.; Shi, H.; Kaviratna, P. D. In Nanotechnology; Chow, G. M.; Gonsalves, K. E., Eds.; ACS Symposium Series 622, American Chemical Society: Washington, DC, 1996; p 251.
10. Giannelis, E. P. Adv Mater 1996, 8, 29.
11. Lagaly, G. In Development in Ionic Polymers; Wilson, A. D.; Posser, H. T., Eds.; Applied Science: London, 1986; Chapter 2, p 77.
12. Pinnavaia, T. J.; Lan, T.; Wang, Z.; Shi, H.; Kaviratna, P. D. Polym Mater Sci 1995, 73, 296.
13. Kelly, P.; Akelah, A.; Qutubuddin, S.; Moet, A. J Mater Sci 1994, 29, 2274.
14. (a) Kojima, Y.; Usuki, A.; Kawasumi, M.; Fukushima, Y.; Okada, A.; Kurauchi, T.; Kamigaito, O. J Polym Sci A Polym Chem 1993, 31, 2493. (b) Reichert, P.; Kressler, J.; Thomann, R.; Mülhaupt, R.; Stöppelmann, G. Acta Polym 1998, 49, 116–123.
15. Usuki, A.; Kato, M.; Okada, A.; Kurauchi, T. J. J Appl Polym Sci 1996, 63, 137.
16. (a) Kawasumi, M.; Hasegawa, N.; Kato, M.; Usuki, A.; Okada, A. Macromolecules 1997, 30, 6333–6338. (b) Hasegawa, N.; Kawasumi, M.; Kato, M.; Usuki, A.; Okada, A. J Appl Polym Sci 1998, 67, 87.
17. Lee, D. C.; Jang, L. W. J Appl Polym Sci 1996, 61, 1117.
18. Biasci, L.; Aglietto, M.; Ruggeri, G.; Ciardelli, F. Polymer 1994, 35, 3296–3304.
19. Biasci, L.; Aglietto, M.; Ruggeri, G.; D'Alessio, A. Polym Adv Tech 1995, 6, 662–670.
20. Smoug, D. Mod Plast 1998, 2, 28.
21. Usuki, A.; Koiwai, A.; Kojima, Y.; Kawasumi, M.; Okada, A.; Fukushima, Y.; Kurauchi, T.; Kamigaito, O. J Mater Res 1993, 49, 1259.
22. Lvov, Y.; Ariga, K.; Ichinose, I.; Kunitake, T. Langmuir 1996, 12, 3038–3044.
23. Bar, G.; Thomann, Y.; Brandsch, R.; Cantow, H.-J.; Whangbo, M. H. Langmuir 1997, 13, 3807–3812.